



# Real-time chatter detection via iterative Vold-Kalman filter and energy entropy

Xingjian Dong<sup>1</sup> · Guowei Tu<sup>1</sup> · Xiaoshan Wang<sup>2</sup> · Shiqian Chen<sup>3</sup>

Received: 10 March 2021 / Accepted: 16 June 2021 / Published online: 6 July 2021

© The Author(s), under exclusive licence to Springer-Verlag London Ltd., part of Springer Nature 2021

## Abstract

Real-time chatter detection is important in improving the surface quality of workpieces in milling. Since the process from stable cutting to chatter is characterized by the progressive variation of the vibration energy distribution, entropy has been utilized to capture the decreasing randomness of vibration signals when chatter occurs. To make such an index more sensitive to transitions of the cutting state, the entropy can be computed based on signal components obtained through signal decomposition techniques. However, the classic empirical mode decomposition (EMD) is difficult to put into practice due to its weak robustness to noises. The up-to-date variational mode decomposition (VMD) has strict requirements on a priori information about the signal and thus is not applicable either. In this paper, a novel method named the iterative Vold-Kalman filter (I-VKF) is proposed under the framework of the greedy algorithm, where the Vold-Kalman filter (VKF), a classic order tracker for rotating machinery, is improved to recursively extract each signal component. In the meantime, a spectrum concentration index-based technique is developed for the estimation of the instantaneous chatter frequency to adaptively determine the filter parameter. Numerical examples demonstrate the superiority of the I-VKF over the original VKF, EMD, and VMD, especially in the presence of strong noises. Combined with the energy entropy of extracted components and an automatically calculated threshold, the proposed strategy greatly helps in timely chatter detection, which has been verified by dynamic simulation and experiments.

**Keywords** Chatter detection · Signal decomposition · Empirical mode decomposition · Vold-Kalman filter · Energy entropy

## 1 Introduction

Chatter is a type of unexpected self-excited vibration occurring in almost all machining processes, which limits the

productivity, damages the machined surface, and shortens the tool life [1]. With the development of automation, the flexibility of the machine tool leads to diverse working conditions in milling processes. Therefore, it is impossible to completely avoid chatter. Over the past decades, researchers devote their efforts to chatter prediction before milling. They focus on the stability lobe chart based on the identified dynamic model of the milling system [2]. Nonetheless, chatter may still occur when machining under stable conditions indicated by theoretical prediction, because the lobe chart is sensitive to the system parameters that are uncertain in engineering.

Real-time chatter detection is an online approach necessitating the least a priori information on the milling system. Combined with the subsequent controlling operation, this strategy helps to eliminate chatter in time. In real-time chatter detection, various signals are collected to provide substantial information, including the cutting force [3], spindle acceleration [4], spindle torque [5], workpiece displacement [6], and machining noise [7]. Signal processing methods are applied then to extract the crucial feature, and the corresponding

---

✉ Xingjian Dong  
donxij@sjtu.edu.cn

Guowei Tu  
guoweitu@sjtu.edu.cn

Xiaoshan Wang  
xiaoshan.wang@jaka.com

Shiqian Chen  
chenshiqian@swjtu.edu.cn

<sup>1</sup> State Key Laboratory of Mechanical System and Vibration, School of Mechanical Engineering, Shanghai Jiao Tong University, Shanghai 200240, China

<sup>2</sup> Shanghai JAKA Robotics Co. Ltd., Shanghai 201100, China

<sup>3</sup> State Key Laboratory of Traction Power, Southwest Jiaotong University, Chengdu 610031, China

cutting state indicator can be established. The effectiveness of such an indicator is the key to achieve the chatter prognosis at an early stage.

Characterizing the variation in the vibration energy distribution from stable cutting to chatter, entropy-based indicators are widely used, such as the approximate entropy [8] and multiscale entropy [9] in the time domain, and the normalized spectral entropy [10] and spectral Rényi entropy [11] in the frequency domain. However, these indices fail to reflect the cutting state timely when raw data are analyzed, because the complexity of milling responses reduces their sensitivity. Under such a circumstance, signal decomposition techniques are utilized as a pre-processor to decompose the original signal into a series of simple intrinsic components. Although the well-known empirical mode decomposition (EMD) [12] has been applied [13], the lack of a rigorous mathematical foundation makes this classic method extremely sensitive to noise and thus difficult to put into practice. The later developed variational mode decomposition (VMD) [14] outperforms the EMD in robustness but requires the number of signal components as a priori parameter [15], which is difficult to obtain in engineering. Moreover, nonlinearity and time-delay in milling systems result in the wideband property of milling responses [16, 17]. Therefore, when the narrowband filter bank-based approaches like the VMD and empirical wavelet transform (EWT) [18] are applied, the obtained signal components tend to be physically meaningless [19–21].

In real-time condition monitoring of rotating equipment, the Vold-Kalman filter (VKF) [22] is of great importance. Strong robustness and low computational cost are achieved thanks to the framework of the widely used Kalman filter [23]. As a tachometer measurement-based order tracker [22], the VKF simultaneously extracts all the order-based harmonic components from measured vibration responses, which characterize tooth-passing dynamics in milling processes. However, when chatter occurs, non-harmonic modes become the main concern, and thus, the order-tracking is no longer helpful [24]. This is because the chatter signal can only be effectively decomposed with the information about the instantaneous chatter frequency. In the meanwhile, as machining dynamics become more complex and the number of signal components increases, the joint optimization (i.e., the simultaneous extraction of all the components) in the VKF tends to be computationally unstable [25]. That being the case, the framework of the VKF needs to be improved and the accurate instantaneous frequency (IF) of each chatter mode is required to adaptively determine the filter parameter.

In this work, based on the spectrum concentration index (SCI) [26], a measure to evaluate the degree of signal demodulation, a novel technique is developed to parametrically estimate the signal IF. This technique transforms the estimation of a continuous IF into the optimization of a few polynomial coefficients, and thus works effectively even in the presence

of strong noises. With this approach, only the IF of the dominant mode with the highest energy in the signal can be obtained. Therefore, under the framework of the greedy algorithm, the original VKF is modified to recursively extract each component based on the latest available IF information, just like the EMD does [12]. As a result, the number of components is automatically determined and the filter becomes more stable and more adaptive compared to the original VKF. The procedures above lead to a new multicomponent signal decomposition tool named the iterative Vold-Kalman filter (I-VKF). A numerical example is given to demonstrate the superiority of the I-VKF over the EMD, VMD, and original VKF. Then, the energy entropy [27], a generalization of Shannon's entropy [28] in the energy domain, is computed based on extracted signal components to capture the decreasing randomness [29] of vibration responses when chatter occurs. Based on collected stable milling responses, the chatter alarm threshold of the entropy is set by the maximum likelihood estimation [30] and the three-sigma criterion [31]. Using the developed strategy, chatter can be detected accurately and timely, which has been demonstrated by dynamic simulation and experimental verification.

The remainder of this paper is organized as follows. The proposed iterative Vold-Kalman filter is detailed in Section 2. Section 3 introduces the energy entropy as the cutting state indicator. Section 4 presents dynamic simulation to demonstrate the effectiveness of the proposed method. In Section 5, the procedure for determining the threshold is given. Section 6 describes the detailed implementation of the online strategy and several milling experiments conducted. Section 7 concludes this paper.

## 2 Iterative Vold-Kalman filter

### 2.1 Chatter frequency estimation based on spectrum concentration index (SCI)

The complex dynamic response  $s(t)$  measured during milling processes can be regarded as a superposition of multiple single modes as

$$s(t) = \sum_{j=1}^N s_j(t), \quad (1)$$

where the  $j$ th mode  $s_j(t)$  is parametrically modeled here as a polynomial phase signal as

$$s_j(t) = a_j(t) \exp \left( \sqrt{-1} \left( 2\pi \left( c_0 t + \sum_{i=1}^k \frac{c_i}{i+1} t^{i+1} \right) + \varphi_0 \right) \right), \quad (2)$$

where  $a_j(t)$  is the amplitude,  $c(t) = \sum_{i=0}^k c_i t^i$  stands for the IF

of the mode,  $k$  is the order of the polynomial phase,  $c_0$  represents the initial frequency,  $c_i (i = 1, \dots, k)$  denotes IF parameters, and  $\varphi_0$  is the initial phase. In this manner, the estimation of the continuous IF is equivalent to the estimation of polynomial parameters, which greatly simplifies the problem. If the term  $\sum_{i=1}^k c_i t^{i+1} / (i + 1)$  is removed from the polynomial, the energy of  $s_j(t)$  will concentrate on  $c_0$  in the frequency domain; that is, the signal mode  $s_j(t)$  will be fully demodulated. As a result, a demodulation operator can be defined as

$$\Phi(t; \tilde{\mathbf{C}}) = \exp\left(-(\sqrt{-1})2\pi \sum_{i=1}^k \frac{\tilde{c}_i}{i+1} t^{i+1}\right), \tag{3}$$

where  $\tilde{\mathbf{C}} = \{\tilde{c}_1, \tilde{c}_2, \dots, \tilde{c}_k\}$  are the estimated IF parameters. Then, the demodulated mode can be obtained as

$$s_{j,d}(t; \tilde{\mathbf{C}}) = s_j(t)\Phi(t; \tilde{\mathbf{C}}). \tag{4}$$

When the estimated IF is exactly the true one (i.e.,  $\tilde{\mathbf{C}} = \mathbf{C}$ ), the signal is fully demodulated as

$$s_{j,d}(t; \mathbf{C}) = a_j(t)\exp(\sqrt{-1}(2\pi c_0 t + \varphi_0)), \tag{5}$$

where the spectrum has a single peak at the constant frequency  $c_0$ . Following this idea, the SCI is adopted to evaluate the spectrum concentration degree of the demodulated signal as [26]

$$SCI(\tilde{\mathbf{C}}) = E\left(\left|\mathcal{F}\left(s_{j,d}(t; \tilde{\mathbf{C}})\right)\right|^4\right), \tag{6}$$

where  $E(\cdot)$  stands for the expectation and  $\mathcal{F}(\cdot)$  denotes the Fourier transform. The optimized  $\tilde{\mathbf{C}}$  can be expressed as

$$\tilde{\mathbf{C}}_{\text{opt}} = \left\{\tilde{c}_1, \tilde{c}_2, \dots, \tilde{c}_k\right\}_{\text{opt}} = \underset{\tilde{\mathbf{C}}}{\text{argmax}} \text{SCI}(\tilde{\mathbf{C}}), \tag{7}$$

and then  $\tilde{c}_0$  can be naturally worked out as

$$\tilde{c}_0 = \underset{f}{\text{argmax}} \left|\mathcal{F}\left(s_{j,d}(t; \tilde{\mathbf{C}}_{\text{opt}})\right)\right|, \tag{8}$$

i.e., the peak frequency in the Fourier spectrum of the demodulated modes  $s_{j,d}$ , and this frequency can be easily detected. A modified particle swarm optimization with dynamic adaptation (DAPSO), of which the ability to jump out of the local extrema is greatly improved and the convergence is accelerated compared with the original PSO [32], is adopted to solve the nonlinear optimization problem in Eq. (7) [33]. The size of the population is set to 30 and the initial values are set as zero in this work. Obtaining the  $\tilde{\mathbf{C}}$  and  $\tilde{c}_0$  through Eqs. (7) and (8), the IF of the target mode  $s_j(t)$  can be accurately estimated. Since the SCI is to be maximized, the IF of the

strongest mode with the highest energy in the synthetic signal will be estimated first.

### 2.2 Signal decomposition via iterative Vold-Kalman filter (I-VKF)

With the estimated IF, the VKF can be employed to extract the target component  $s_j(t)$ . The center frequency for the VKF can be adjusted adaptively according to the estimated IF, which makes it possible to separate closely distributed or even crossed signal modes in the time-frequency plane. However, in the original VKF, the tachometer information has to be collected and a joint optimization is adopted (i.e., all the components are simultaneously extracted) [22], while by using the approach in Section 2.1, only the IF of the dominant mode with the highest energy can be obtained. Therefore, the VKF is modified in this work under the framework of the greedy algorithm to recursively extract each component.

The mode  $s_j(t)$  in model (1) can be given in another form as

$$s_j(t) = a_j(t)\Theta_j(t), \tag{9}$$

where  $a_j(t)$  represents the amplitude envelope and  $\Theta_j(t)$  denotes the carrier signal as

$$\Theta_j(t) = \exp\left(\sqrt{-1}\int_0^t \omega_j(\tau) d\tau\right), \tag{10}$$

where  $\int_0^t \omega_j(\tau) d\tau$  denotes the instantaneous phase with  $\omega_j(\tau)$  being the instantaneous circular frequency. In the original VKF [22], it is assumed that  $\omega_j(\tau)$  is an integer or fractional multiple of the fundamental frequency (i.e., the spindle rotational frequency), but this assumption is not made here. Target components are no longer limited to the order-based harmonics.

For discrete signals, the smooth degree of the slowly varying amplitude function  $a_j(t)$  can be evaluated by

$$\nabla^s \mathbf{a}_j(m) = \varepsilon_j(m), \quad m = 1, 2, \dots, M, \tag{11}$$

where  $s$  is the difference order,  $\nabla$  denotes the difference operator,  $M$  is the signal length, and  $\varepsilon_j$  stands for the higher order term. Setting  $s = 2$  (i.e., the second-order VKF is employed), Eq. (11) can be formulated as

$$\mathbf{a}_j(m-1) - 2\mathbf{a}_j(m) + \mathbf{a}_j(m+1) = \varepsilon_j(m), \tag{12}$$

where  $\mathbf{a}_j(0) = 0$  and  $\mathbf{a}_j(M+1) = 0$  for a practical causal signal. The matrix form of Eq. (12) is given as

$$\begin{bmatrix} -2 & 1 & 0 & \dots & 0 \\ 1 & -2 & 1 & \dots & 0 \\ 0 & 1 & -2 & \dots & \vdots \\ \vdots & \vdots & \vdots & \ddots & 1 \\ 0 & 0 & \dots & 1 & -2 \end{bmatrix} \begin{bmatrix} \mathbf{a}_j(1) \\ \mathbf{a}_j(2) \\ \mathbf{a}_j(3) \\ \dots \\ \mathbf{a}_j(M) \end{bmatrix} = \begin{bmatrix} \varepsilon_j(1) \\ \varepsilon_j(2) \\ \varepsilon_j(3) \\ \vdots \\ \varepsilon_j(M) \end{bmatrix}. \tag{13}$$

Equation (13) can be written as

$$\mathbf{R}\mathbf{a}_j = \boldsymbol{\varepsilon}_j, \tag{14}$$

which is the *structural equation* corresponding to the *state equation* in the Kalman filter [23]. In the meanwhile, the measured signal  $s(t)$  in Eq. (1) can be re-formulated in a discrete form as

$$\mathbf{s}(m) = \mathbf{a}_j(m)\boldsymbol{\Theta}_j(m) + \boldsymbol{\xi}_j(m), \quad m = 1, 2, \dots, M. \tag{15}$$

Note that in the original VKF [22], all the components are jointly estimated and  $\boldsymbol{\xi}_j(m)$  in Eq. (15) only includes the estimation error and noise, while in this work  $\boldsymbol{\xi}_j(m)$  also includes the non-target components (i.e.,  $\mathbf{s}_p(m), p = 1, 2, \dots, N, p \neq j$ ). Such an idea coincides with the greedy algorithm; that is, the non-target components are regarded as the unwanted noise, and the target component is extracted *greedily* in each round of optimization. In other words, the obtained mode in each extraction takes away as much energy as possible from the current signal. This strategy is effective because it is consistent with the technique of the chatter frequency estimation developed in Section 2.1, where only the IF of the dominant mode is estimated. Finally, all the extractions together formulate the signal decomposition. Equation (15) can be expressed in the form of a matrix equation as

$$\begin{bmatrix} \mathbf{s}(1) \\ \mathbf{s}(2) \\ \vdots \\ \mathbf{s}(M) \end{bmatrix} - \begin{bmatrix} \boldsymbol{\Theta}_j(1) & 0 & \cdots & 0 \\ 0 & \boldsymbol{\Theta}_j(2) & \cdots & 0 \\ \vdots & \vdots & \ddots & \vdots \\ 0 & 0 & \cdots & \boldsymbol{\Theta}_j(M) \end{bmatrix} \begin{bmatrix} \mathbf{a}_j(1) \\ \mathbf{a}_j(2) \\ \vdots \\ \mathbf{a}_j(M) \end{bmatrix} = \begin{bmatrix} \boldsymbol{\xi}_j(1) \\ \boldsymbol{\xi}_j(2) \\ \vdots \\ \boldsymbol{\xi}_j(M) \end{bmatrix}, \tag{16}$$

which can also be written as

$$\mathbf{s} - \mathbf{B}_j \mathbf{a}_j = \boldsymbol{\xi}_j. \tag{17}$$

Similarly, Eq. (17) is a variant of the *data equation* corresponding to the *measurement equation* in the Kalman filter [23].

Combining the structural equation (14) and the data equation (17), a weighted loss function  $\mathcal{L}$  in the sense of  $\ell^2$  norm is given as

$$\mathcal{L} = \lambda^2 \|\boldsymbol{\varepsilon}_j\|_2^2 + \|\boldsymbol{\xi}_j\|_2^2 = \lambda^2 \boldsymbol{\varepsilon}_j^H \boldsymbol{\varepsilon}_j + \boldsymbol{\xi}_j^H \boldsymbol{\xi}_j, \tag{18}$$

where  $\lambda$  is a weighting factor and the superscript H denotes the conjugate transpose. To minimize the function  $\mathcal{L}$ , the normal equation is introduced as

$$\frac{\partial \mathcal{L}}{\partial \mathbf{a}_j} = (\lambda^2 \mathbf{R}^T \mathbf{R} + \mathbf{I}) \mathbf{a}_j - \mathbf{B}_j^H \mathbf{s} = \mathbf{0}, \tag{19}$$

where  $\mathbf{I}$  denotes the identity matrix. Equation (19) leads to the optimal solution for  $\mathbf{a}_j$  as

$$\tilde{\mathbf{a}}_j = (\lambda^2 \mathbf{R}^T \mathbf{R} + \mathbf{I})^{-1} \tilde{\mathbf{B}}_j^H \mathbf{s} \triangleq \mathbf{G}^{-1} \tilde{\mathbf{B}}_j^H \mathbf{s}. \tag{20}$$

The target mode  $\mathbf{s}_j$  can be finally reconstructed as

$$\tilde{\mathbf{s}}_j = \tilde{\mathbf{B}}_j \tilde{\mathbf{a}}_j, \tag{21}$$

where the square matrix  $\tilde{\mathbf{B}}_j$  can be easily formulated because the  $\omega_j(\tau)$  in Eq. (10) has been worked out with the estimated IF. Thanks to the sparsity of matrix  $\mathbf{G}$  in Eq. (20), the Cholesky factorization of matrix  $\mathbf{G}$  [34] can be employed as the fastest algorithm to solve Eq. (19). Besides, the weighting factor  $\lambda$  is set to  $1 \times 10^6$  in this work to achieve a trade-off between the accuracy and computational cost [25].

Thus far, the entire I-VKF method can be summarized in Fig. 1. The extraction of signal modes is implemented recursively until the residual energy ratio is less than a pre-set value (5% is used here); that is, the mode number  $N$  is determined automatically. Considering that the mode number (i.e., the highest order) is empirically specified in the original VKF, the improved framework makes the filter more adaptive. Besides, the recursive decomposition rather than simultaneous extraction makes the filter more stable, which will be verified by the following example.

### 2.3 An example

To validate the proposed method, an example of a four-component signal is given as

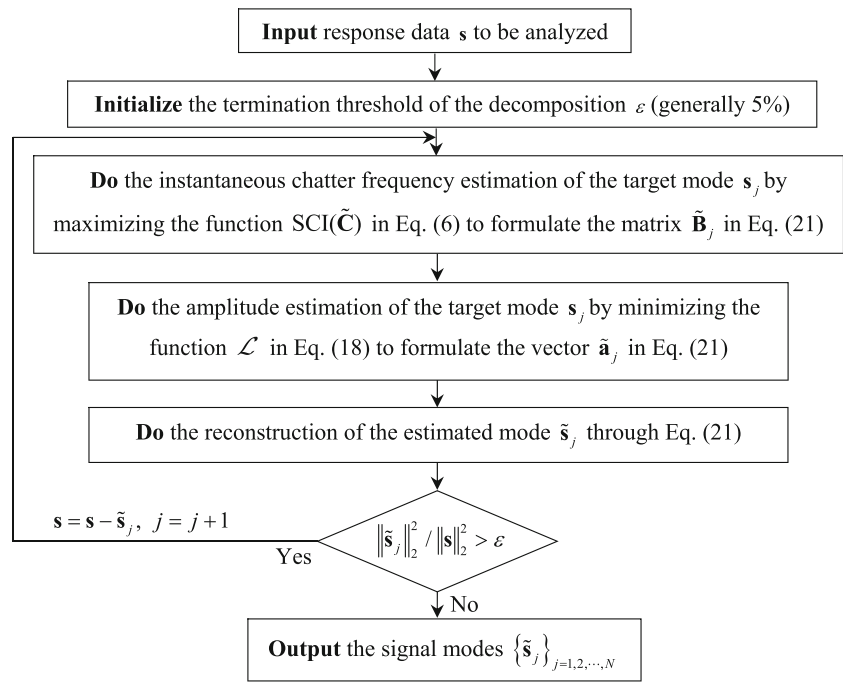
$$\begin{cases} s(t) = s_1(t) + s_2(t) + s_3(t) + s_4(t), & 0 \leq t \leq 15 \text{ s}, \\ s_1(t) = \exp(-0.1t) \cos(2\pi(5t)), \\ s_2(t) = \exp(-0.1t) \cos\left(2\pi\left(10t + 1.5t^2 - \frac{1}{30}t^3\right)\right), \\ s_3(t) = \exp(-0.1t) \cos\left(2\pi\left(20t + 1.8t^2 - \frac{1}{20}t^3\right)\right), \\ s_4(t) = \exp(-0.1t) \cos\left(2\pi\left(40t + 0.5t^2 - \frac{1}{15}t^3\right)\right), \end{cases} \tag{22}$$

where IFs of four modes are  $f_1(t) = 5, f_2(t) = 10 + 3t - 0.1t^2, f_3(t) = 20 + 3.6t - 0.15t^2$ , and  $f_4(t) = 40 + t - 0.2t^2$  respectively.

The signal in Eq. (22) is contaminated by white Gaussian noise with the signal-to-noise ratio (SNR) as 2 dB. The sampling frequency is set to 100 Hz. The waveform of the noisy signal is shown in Fig. 2a. Figure 2c gives the time-frequency representation (TFR) generated by the short-time Fourier transform (STFT), while Fig. 2b is the noise-free version. In the parametric estimation of IFs, the order of the polynomial model is set to three (although true IFs here are of the second-order type).

Table 1 lists the estimated IF parameters by the SCI optimization with corresponding estimation error. Using the I-

**Fig. 1** Flow chart of the developed iterative Vold-Kalman filter (I-VKF)



VKF, extracted four components and their TFRs are shown in Fig. 3. With accurately estimated IFs, four single components are successfully separated and embedded noises are removed. The SNRs of four reconstructed modes are 17.5516 dB, 17.0363 dB, 18.5479 dB, and 16.7213 dB, respectively.

For comparison, decomposition results by the EMD, VMD, and original VKF are also given (note that when the original VKF is used, the number of modes and IF of each mode are taken as known information to initiate the filtering). When the EMD is applied, the strong noise leads to severe mode aliasing [35], as Fig. 4 shows. The filter bank property of the VMD [36] makes obtained single modes physically meaningless as Fig. 5 shows, because four real components, which overlap in the time-frequency domain, cannot be separated by a filter in the frequency domain. When the original VKF is used, four chirp modes are indeed tracked but are distorted by noise (see Fig. 6), which is due to the instability of the joint optimization [25]. Moreover, the computational time consumed by the I-VKF does not exceed that consumed by the VKF (all the tests are carried out with MATLAB®

R2018b on a personal computer with a 3.60-GHz Intel® Core™ i7-7700 CPU).

The above example demonstrates that the developed I-VKF method, which acts as an adaptive time-frequency filter, works effectively in the decomposition of multi-chirp signals with a low SNR, and thus will be of great help in chatter detection.

### 3 Energy entropy-based feature extraction

It is vital to extract the fault feature from measured signals accurately and timely for chatter detection. The selected feature quantity should not only make it simple and feasible for the signal acquisition and data processing but also reflect the essence of milling processes; that is, this quantity should be closely related to the change in cutting states. As an indicator of the internal confusion degree of a system, entropy, such as the permutation entropy [37] and approximate entropy [38], can be expressed as a function of the probability distribution

**Fig. 2** Example of a four-component signal. **a** Waveform of the noisy signal. **b** TFR of the noise-free signal. **c** TFR of the noisy signal. All the TFRs are generated by the STFT

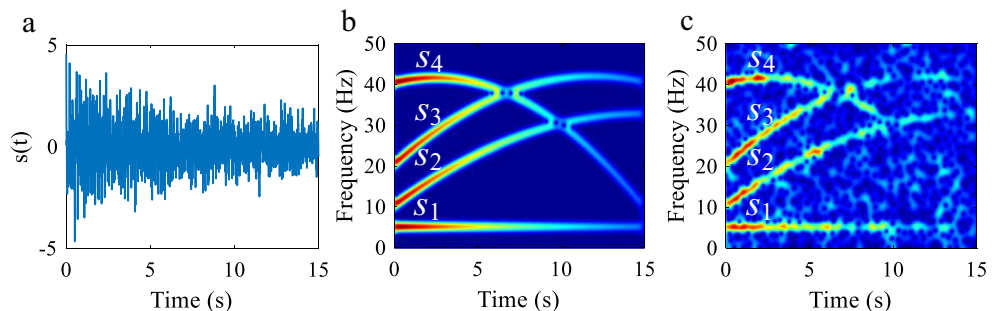




**Table 1** Estimated IF parameters based on the SCI optimization (values in parentheses denote the relative estimation errors)

		$c_0$	$c_1$	$c_2$	$c_3$
$s_1(t)$	Estimated	5.0061	0.0012	0.0004	0.0025
	True	5 (0.12%)	0 (/)	0 (/)	0 (/)
$s_2(t)$	Estimated	9.9930	3.0028	-0.1003	0.0017
	True	10 (0.07%)	3 (0.09%)	-0.1(0.30%)	0 (/)
$s_3(t)$	Estimated	19.9867	3.6047	-0.1503	0.0023
	True	20 (0.07%)	3.6 (0.13%)	-0.15(0.20%)	0 (/)
$s_4(t)$	Estimated	40.0244	0.9978	-0.2006	0.0066
	True	40 (0.06%)	1 (0.22%)	-0.2(0.31%)	0 (/)

of a signal and has been widely applied in fault diagnosis. The energy entropy [27] is utilized in this work to characterize the energy distribution of signal modes  $\{s_1(t), s_2(t), \dots, s_N(t)\}$  of a milling response  $s(t)$ , which are extracted based on the I-VKF approach in Section 2. The energy of each mode is given by

$$E_j = \int |s_j(t)|^2 dt, \quad j = 1, 2, \dots, N. \quad (23)$$

Neglecting the residual, the aggregate energy of all modes should be equal to that of the original signal. Then, the energy entropy is defined based on Shannon's entropy [28] as

$$H_{\text{energy}} = - \sum_{j=1}^N p_j \log_2 p_j, \quad (24)$$

where  $p_j = E_j/E$  and  $E = \sum_{j=1}^N E_j$ .

Energy entropy in Eq. (24) is a dimensionless index larger than zero. The larger the index, the more dispersed the energy distribution in the frequency domain [27]. Since each mode is located within a specific frequency band, the energy entropy

characterizes the degree of randomness of milling dynamics that underlie a vibration response.

In stable milling, the vibration obeys a Gaussian-like distribution in the time domain and shows a wideband property in the frequency domain. At an early stage of chatter, the amplitudes at certain frequencies (i.e., chatter frequency and its harmonics) gradually increase, and the vibration energy tends to gather within several narrow bands. As chatter becomes more severe, the vibration resembles a sinusoidal oscillation, which results in a rapid decrease in signal randomness in the time domain.

According to the above mechanism, a strategy is proposed for chatter detection, which combines the I-VKF-based decomposition in Section 2 and the energy entropy-based feature extraction in Section 3. In this way, the progressive change in cutting states can be accurately captured by the energy entropy that is computed based on signal modes extracted from milling responses. The effectiveness of this strategy will be demonstrated by dynamic simulation and experiments in Section 4 and Section 6, respectively.

## 4 Dynamic simulation

In this section, milling vibration responses are simulated using the Runge-Kutta algorithm. The classic Balachandran two-degree-of-freedom milling model [39] is considered and the simulation parameters follow those in the original investigation [39]. We give two cases where the spindle speed and the axial cutting depth linearly increase, respectively. As Fig. 7 shows, the process from stable cutting to chatter can be observed in both cases, and the corresponding transition points A, B, and C coincide with those predicted by the stability lobe [39].

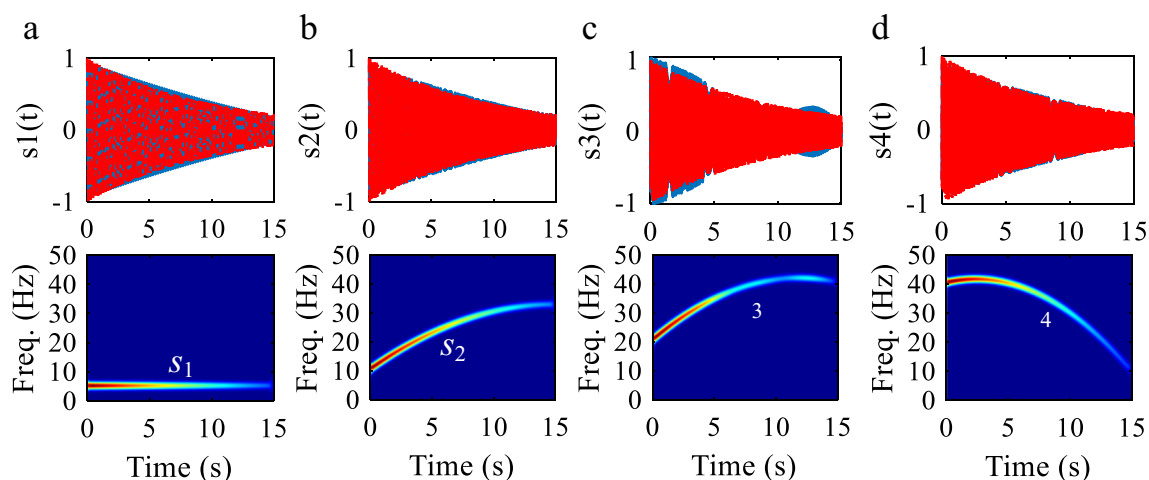


**Fig. 3** Extracted components by the I-VKF. **a–d** give  $s_1 \sim s_4$  respectively. Top panels are waveforms (blue lines denote the estimated ones while red lines denote the true ones). Bottom panels are corresponding TFRs generated by the STFT

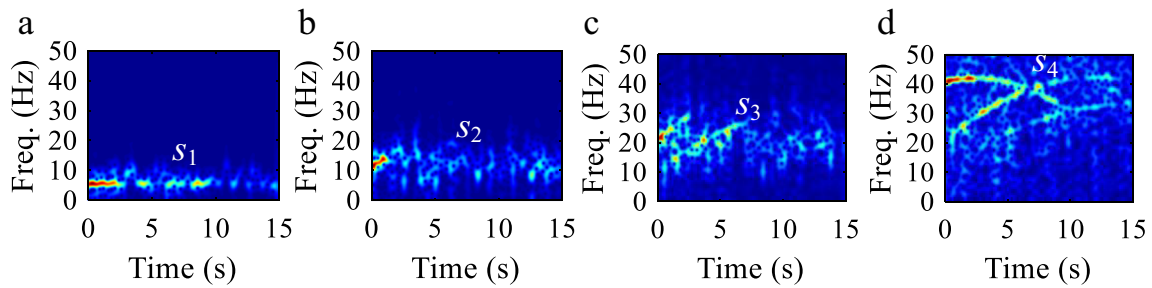


Fig. 4 Extracted components by the EMD. a–d give TFRs of  $s_1 \sim s_4$  generated by the STFT respectively

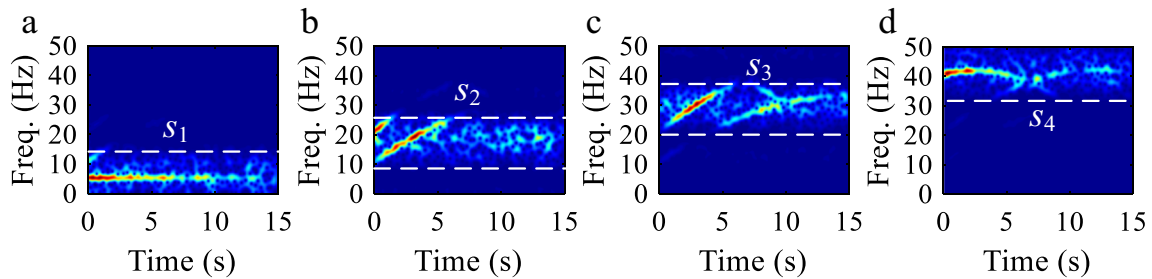


Fig. 5 Extracted components by the VMD. a–d give TFRs of  $s_1 \sim s_4$  generated by the STFT respectively

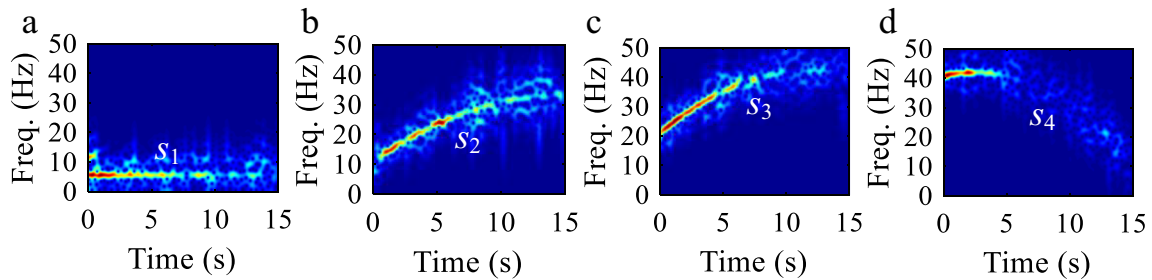
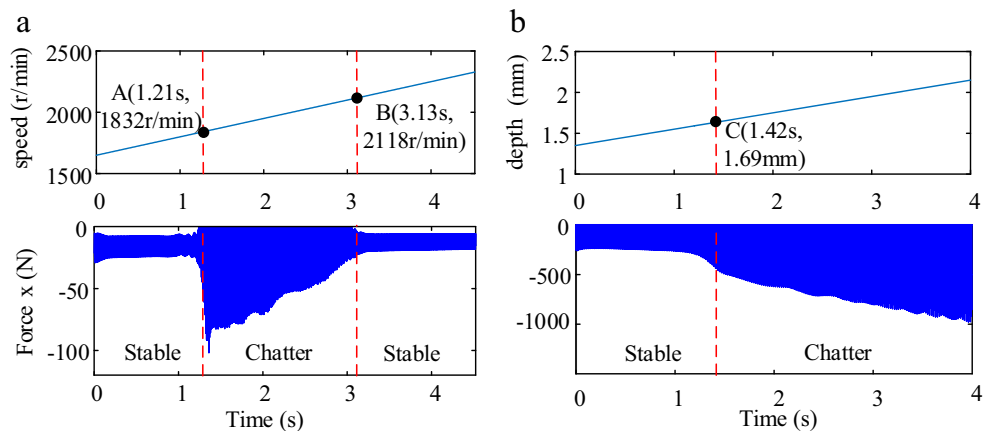


Fig. 6 Extracted components by the original VKF. a–d give TFRs of  $s_1 \sim s_4$  generated by the STFT respectively

Fig. 7 Two simulation cases. a Case #1 with linearly increasing spindle speed. b Case #2 with linearly increasing axial cutting depth. Top panels denote the variations of the processing parameters and bottom panels denote the milling force responses in the feed direction



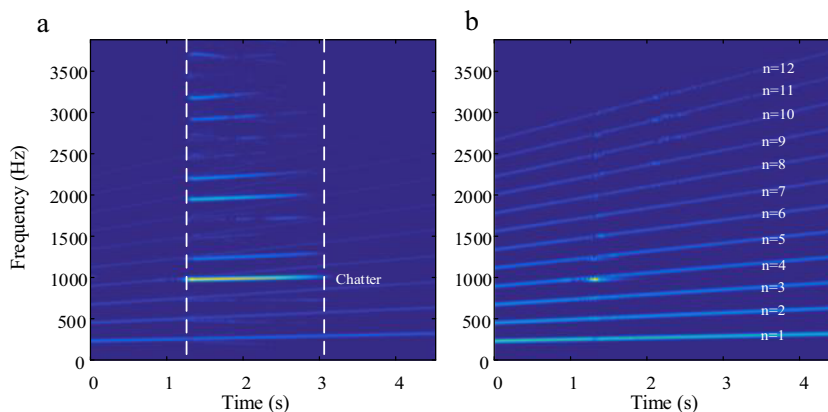
A preliminary time-frequency analysis of the response in case #1 is given in Fig. 8a. The force signal consists of three types of components: the tooth-passing modes resulting from spindle rotations, random modes due to system noises, and chatter modes caused by *regenerative effects* [40], which together lead to an intricate spectrum.

Since the spindle speed is known, the VKF is applied as a pre-processor to remove the tooth-passing components before the decomposition, with the aim to eliminate the interference of spindle rotations and intermittent cutting. The TFR of the components filtered out is shown in Fig. 8b. The remaining signal is then decomposed by the I-VKF into eight modes as Fig. 9 shows (note that in all the following simulated and experimental cases, only the third-order polynomial model is considered in the SCI optimization to minimize the computational cost). The energy of the extracted mode reduces as the order increases, which is consistent with the idea of the greedy algorithm. Eight modes exhibit chatter-related dynamics, showing the chatter frequencies that are spindle speed-independent [40]. Similar characteristics can be observed when the same processing is applied to the response in case #2.

The VMD and EMD are also applied to decompose the milling force signal and the results are given in Fig. 10 and Fig. 11, respectively. Mode aliasing can be observed in eight components extracted by the VMD and this problem is even exacerbated when the EMD is used, which makes the introduction of the I-VKF technique necessary.

As Fig. 9 shows, TFRs of extracted modes during chatter (the intermediate interval surrounded by two white borders) are much more condensed than those during stable cutting, which suggests a more concentrated energy distribution. This decrease in signal randomness can be captured by the energy entropy that is computed using a sliding window with a length of 0.1 s, as Fig. 12 shows. The energy entropy is sensitive to changes in the cutting state, and the variations of the entropy always precede such changes, which demonstrates the effectiveness of the proposed strategy in timely chatter detection.

**Fig. 8** TFR for case #1. **a** Original simulated force signal. **b** Tooth-passing components filtered out by the VKF



## 5 Threshold determination

Since chatter is expected to be detected automatically, an alarm threshold is needed. In many existing studies, the threshold is determined by manually observing the deviation between index values under chatter and stable cutting [4, 38, 41]. This empirical strategy suffers from the sensitivity to working conditions. In this work, a robust threshold is determined statistically. In many fault diagnosis problems, the fault feature is assumed to obey the Gaussian distribution, which simplifies the model construction for fault classification [42–44]. The same null hypothesis is made here in the analysis of the statistical distribution of milling signals.

At the incipient stage of a machining task, vibration signals under stable cutting can be collected and corresponding energy entropies can be calculated as a sample. Then, the normality test can be carried out on the sample, where the Lilliefors test [45] is adopted in this work because the population mean  $\mu$  and variance  $\sigma^2$  are not known. The statistic is given by

$$D_N = \max_{x \in \mathbb{R}} \left| \hat{F}_N(x) - G_0(x) \right|, \quad (25)$$

where  $x$  is the sample,  $N$  is the sample size,  $\hat{F}_N(x)$  is the empirical cumulative distribution function (CDF) of the sample, and  $G_0(x)$  is the CDF of the hypothesized distribution with the estimated parameters equal to the sample parameters, that is,

$$\begin{cases} \hat{\mu} = \bar{X} = \frac{1}{N} \sum_{k=1}^N X_k, \\ \hat{\sigma}^2 = S^2 = \frac{1}{N-1} \sum_{k=1}^N (X_k - \bar{X})^2. \end{cases} \quad (26)$$

Equation (26) exactly gives the maximum likelihood estimate under a Gaussian distribution [30]. The null hypothesis will be rejected when the observation of  $D_N$  is larger than the critical value at a specified significance level (5% is set here), and this critical value can be obtained by the Monte Carlo method [46].



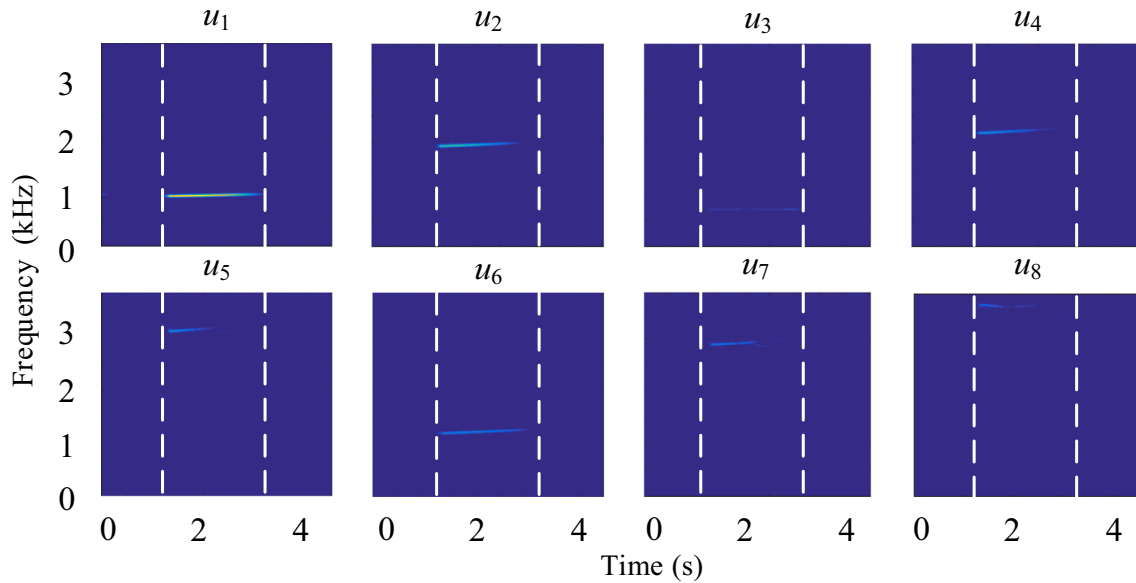


Fig. 9 TFRs of extracted components from the simulated milling force in case #1 by the proposed I-VKF

Once the normality test is approved, the three-sigma criterion [31] will be adopted to calculate the allowable range of the fluctuating energy entropy under stable cutting, which is given by  $[\hat{\mu}-3\hat{\sigma}, \hat{\mu}+3\hat{\sigma}]$ . Considering the decrease in randomness when chatter occurs, the alarm threshold is set as the lower limit, i.e.,  $\hat{\mu}-3\hat{\sigma}$ .

### 6 Implementation and experimental verification

The detailed implementation of chatter detection in the industry is introduced in this section, and a series of milling

experiments are conducted to show the performance of the proposed approach.

#### 6.1 Implementation of chatter detection

Dynamic simulations in Section 4 show promising results of chatter detection based on the I-VKF technique and subsequent energy entropy monitoring. Herein, the practical implementation is given in Fig. 13, which consists of the following steps:

1. Processing parameters' definition: Define the spindle speed, feed rate, and cutting depth. All these parameters can be variable in a milling task.

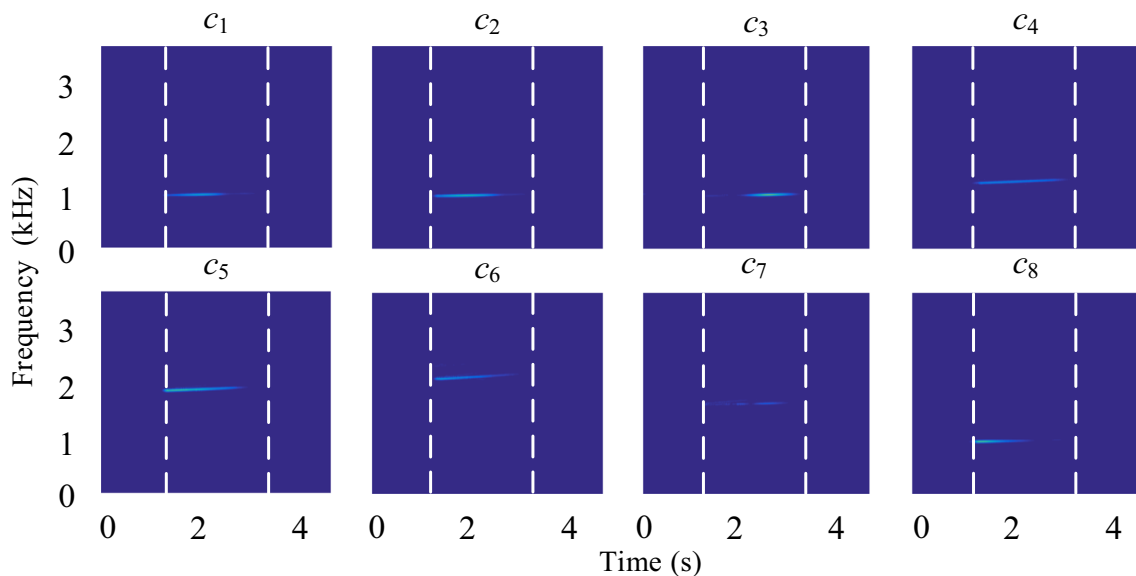


Fig. 10 TFRs of extracted components from the simulated milling force in case #1 by the VMD

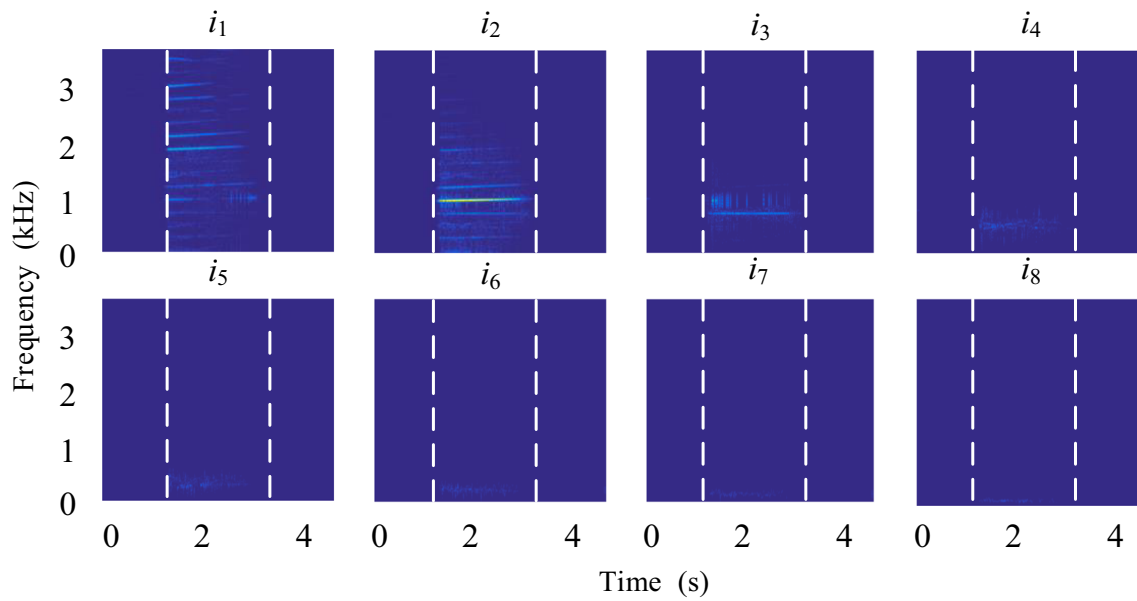


Fig. 11 TFRs of extracted components from the simulated milling force in case #1 by the EMD

2. Vibration signal acquisition: Collect milling system-related vibration signals. The milling force is collected in this work since it suffers from the least influence of

the displacement of transducers [47], but the developed approach can also be utilized to analyze displacement and acceleration signals because the cutting force and vibra-

Fig. 12 Simulated milling force signals with computed energy entropies. a Case #1. b Case #2

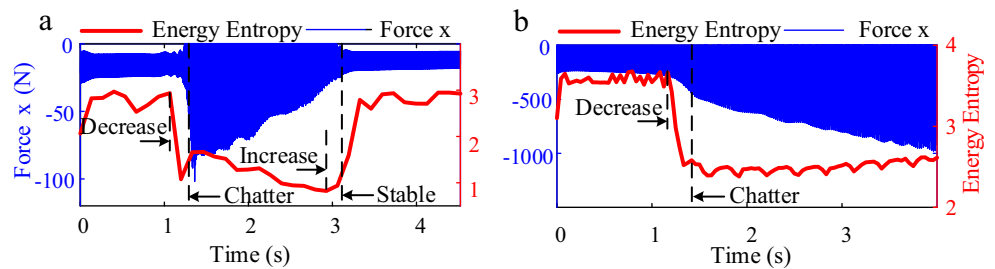
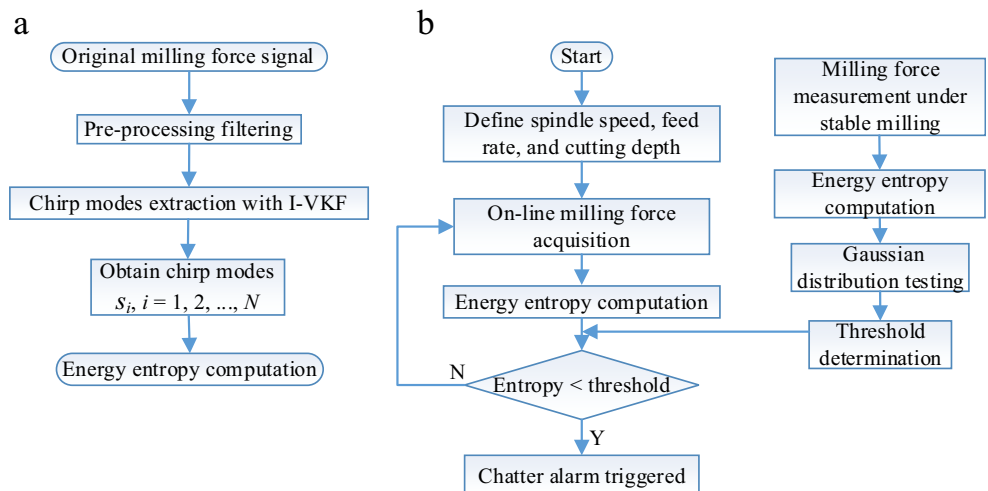


Fig. 13 Implementation of chatter detection. a Flowchart of the energy entropy computation. b Flowchart of the online chatter detection



tion are strongly coupled in milling dynamics; i.e., other types of vibration signals would exhibit the same chatter features [40].

3. Online energy entropy computation: Calculate the real-time energy entropy of the collected signal based on the procedure given in Fig. 13a. A sliding window with a specified window length is used for online monitoring.
4. Threshold determination: Obtain the alarm threshold of the entropy using the incipient stable milling response, according to the strategy in Section 5.
5. Cutting state monitoring: The moment when discrete data points of the computed entropy cross the given threshold three consecutive times triggers the chatter alarm. The situation where only one or two data points cross the threshold and the following point falls back will be regarded as not chatter but an accident.

### 6.2 Experimental setup

The experimental setup is shown in Fig. 14. All the tests were conducted on a DMG five-axis CNC milling machine. The carbon-steel end-milling tool has four teeth and a diameter of 4 mm, and the spindle has an overhang of 40 mm. The workpiece is an aluminum alloy block. The full-immersion cutting was adopted. Chatter vibrations were monitored with a Kistler 9123C dynamometer that was attached to the workpiece. Signals were recorded by a data acquisition card and were analyzed using a PC. The sampling frequency was set to 20 kHz.

The stability of milling is closely related to the spindle speed and depth of cut. Herein, the axial cutting depth varies from 2.6 to 6.7 mm and the spindle speed varies from 3600 to 4200 rpm. Five sets of processing parameters are listed in Table 2. Tests #1–#4 in experiment I give four different

**Table 2** Milling tests with parameters

Experiment	Test	Milling states	$\Omega$ (r/min)	$f$ (mm/min)	$a_p$ (mm)
I	#1	Stable	4200	580	6.6
	#2	Stable	3600	250	2.6
	#3	Chatter	4000	580	6.6
	#4	Severe chatter	4000	640	6.7
II	#5	Stable to chatter	4000	580	6.3

cutting states. Test #5 in experiment II gives a dynamic process from stable cutting to chatter.

### 6.3 Results

#### 6.3.1 Offline experiment I

Four test signals are shown in Fig. 15. In tests #1 and #2, the amplitudes of milling forces are relatively small and the spectra are dominated by the evenly distributed tooth-passing frequencies, which indicates a stable cutting. With an increase in the spindle speed and cutting depth, the slight and the severe chatter occur in tests #3 and #4, respectively, leading to the large amplitudes and conspicuous chatter frequencies that are modulated by the spindle rotational frequency. The uncertainty of the distribution is reduced in these cases. With the I-VKF applied, the single modes of four test signals are obtained and the normalized energy ratios of each mode are calculated and given in Fig. 16a. The results verify the aforementioned Gaussian randomness in stable cutting and the harmonic concentration in chatter. The gathering of energy is also revealed in the computed energy entropies of four test signals, as shown in Fig. 16b.

**Fig. 14** Experimental setup. **a** Picture. **b** Schematic

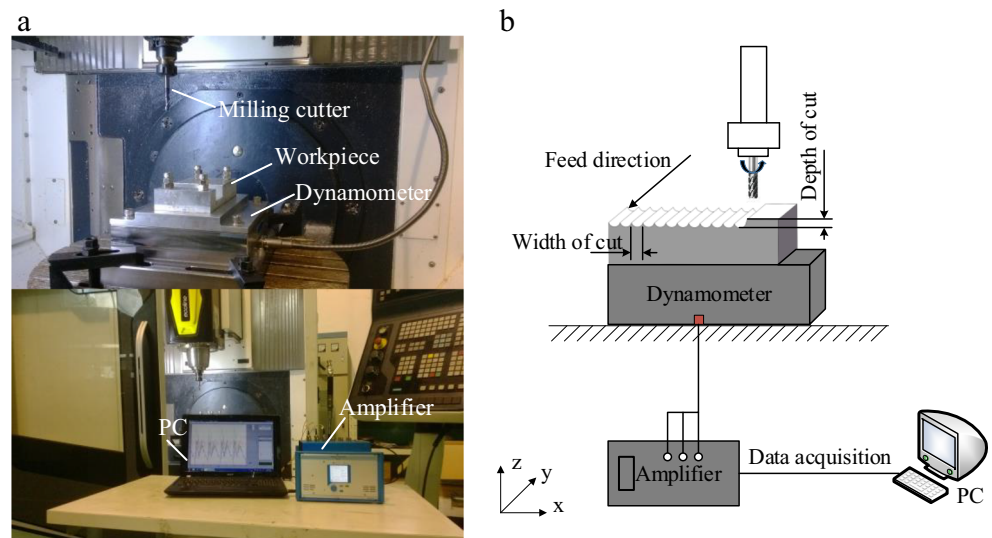


**Fig. 15** Measured milling force signals in the offline experiment I. **a** Temporal waveforms. **b** Fourier spectra (where  $f$  denotes the tooth-passing frequency)

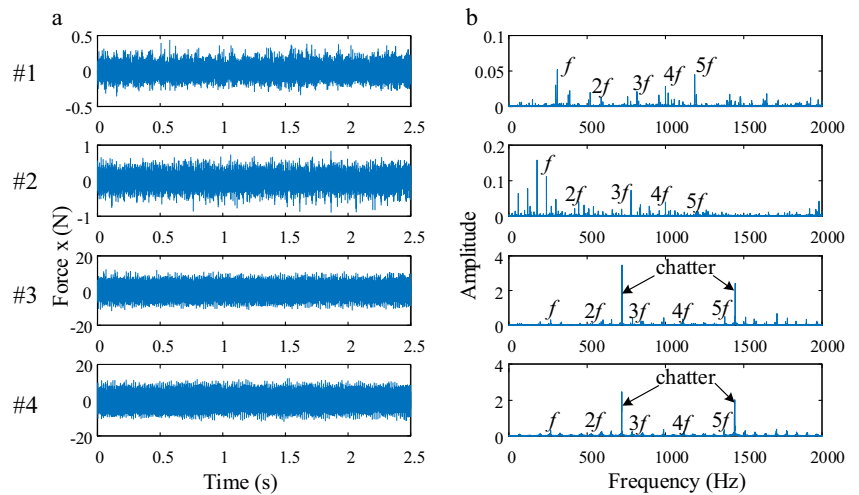
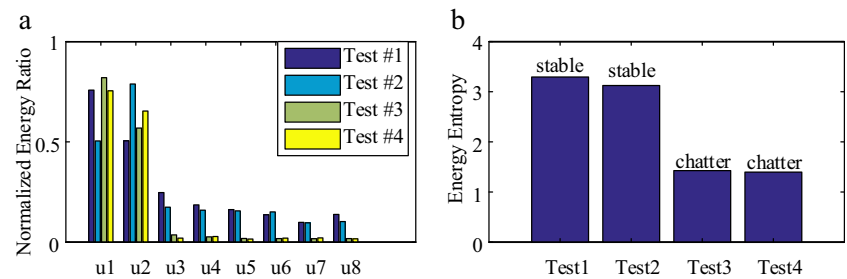


**Fig. 16** Energy distribution of single modes extracted from milling force signals in the offline experiment I. **a** Normalized energy ratio of each mode. **b** Energy entropy of each test signal



The above offline results demonstrate the effectiveness of the proposed method, and the industrial application of this strategy will be further shown in the following online results.

**6.3.2 Online experiment II**

In the second experiment, the cutting state is monitored online. The length of the sliding window is set as 100 points with no overlap. The incipient milling force signals under stable cutting were collected and the corresponding energy entropy was computed. With the Lilliefors test performed, the empirical CDF of the sample versus the theoretical CDF of the hypothesized Gaussian distribution is obtained and given in Fig. 17. The linear regression shows an excellent fit between the two functions. Therefore, the strategy in Section 5 can be used to determine the alarm threshold. The allowable range of the fluctuation is obtained as [2.081, 2.145], and thus, the threshold is set as 2.081.

The collected milling force signal with the corresponding energy entropy computed online is shown in Fig. 18. The indicator detects the premature chatter at  $t = 0.58$  s, around 0.12 s ahead of the moment when the amplitude suddenly increases (which means the destruction of the workpiece). For further verification, the machine was not shut down after the chatter alarm. Three signal samples with an equal duration of 0.3 s marked with S1, S2, and S3 in Fig. 18, respectively,

are extracted and given in Fig. 19. The VKF is applied as a pre-filter to remove the tooth-passing components, and the Fourier spectra after are shown in Fig. 19c.

During the stable cutting (0~0.3 s), the vibration energy disperses within a wide band (see the first panel in Fig. 19c).

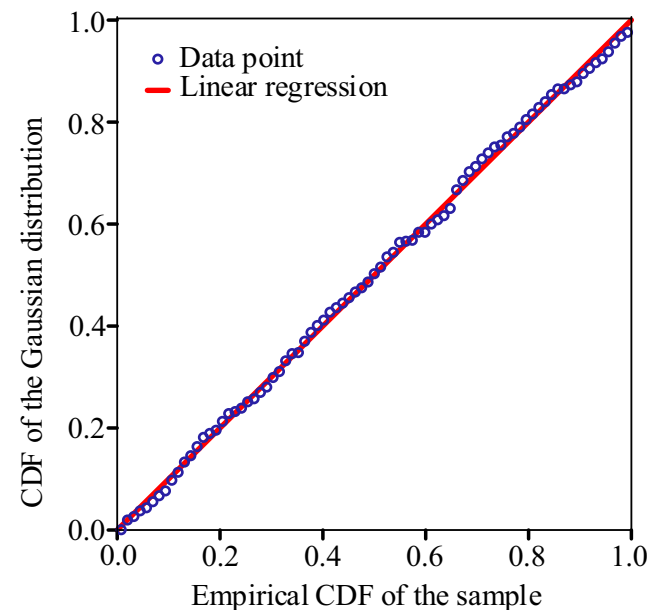
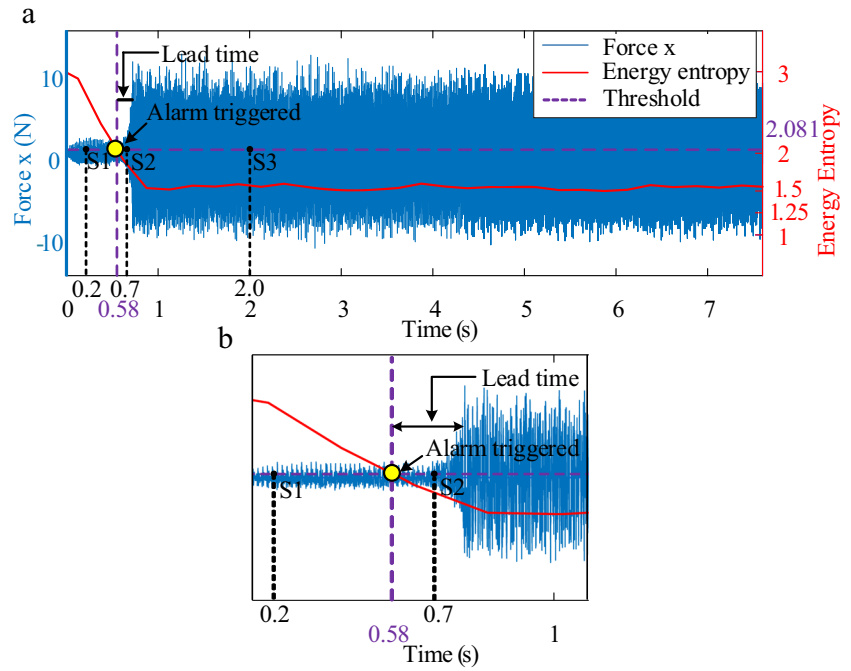


**Fig. 17** The empirical CDF of the sample versus the CDF of the hypothesized Gaussian distribution in the Lilliefors test

**Fig. 18** The collected milling force signal in test #5 with the corresponding energy entropy computed online: (a) Overall view; (b) Local close-up view



With a drastic increase in the vibration amplitude at around 0.6 s, the chatter emerges, which is accompanied by the noticeable chatter frequencies as shown in the second panel in Fig. 19c. At about 1.8 s, chatter has been fully developed. A modulated waveform appears (see the third panel in Fig. 19a)

and the chatter frequencies become dominant, which absorb most of the energy as the third panel in Fig. 19c shows.

The proposed I-VKF and the classic EMD are both applied to decompose the chatter response. As Fig. 20a shows, severe mode aliasing can be observed when the

**Fig. 19** Three signal segments corresponding to S1 (stable), S2 (transition), and S3 (chatter) in Fig. 18 respectively. **a** Temporal waveforms. **b** Original Fourier spectra. **c** Fourier spectra after the VKF filtering (where  $f$  denotes the tooth-passing frequency)

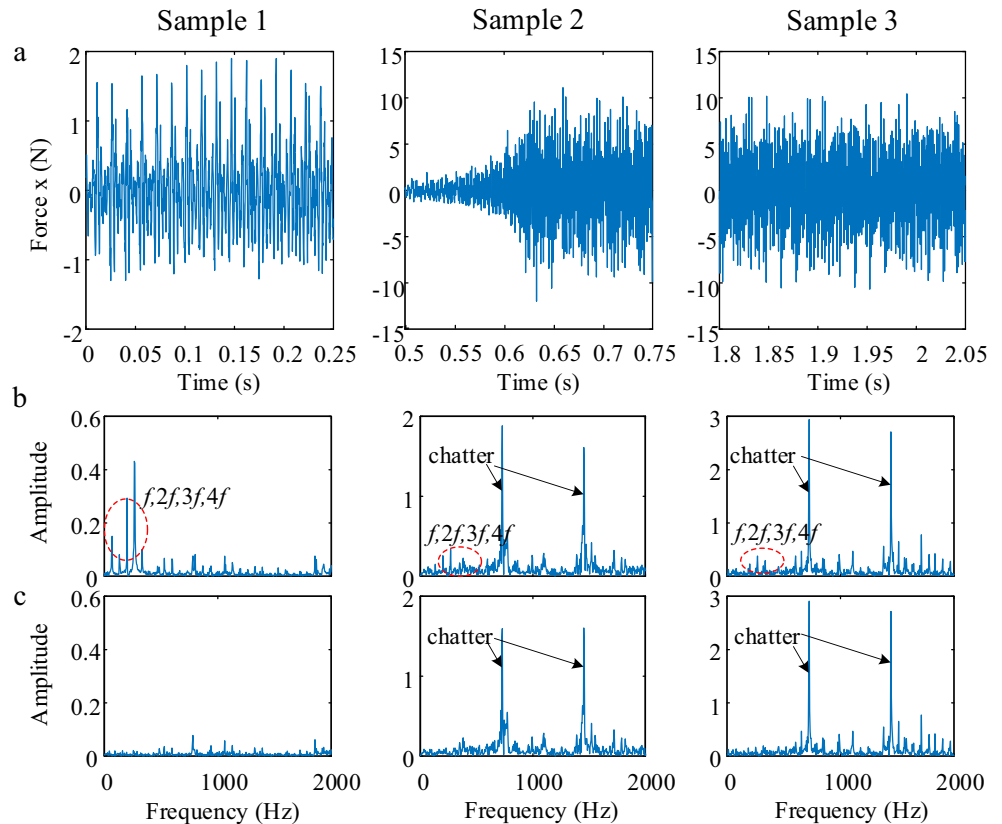
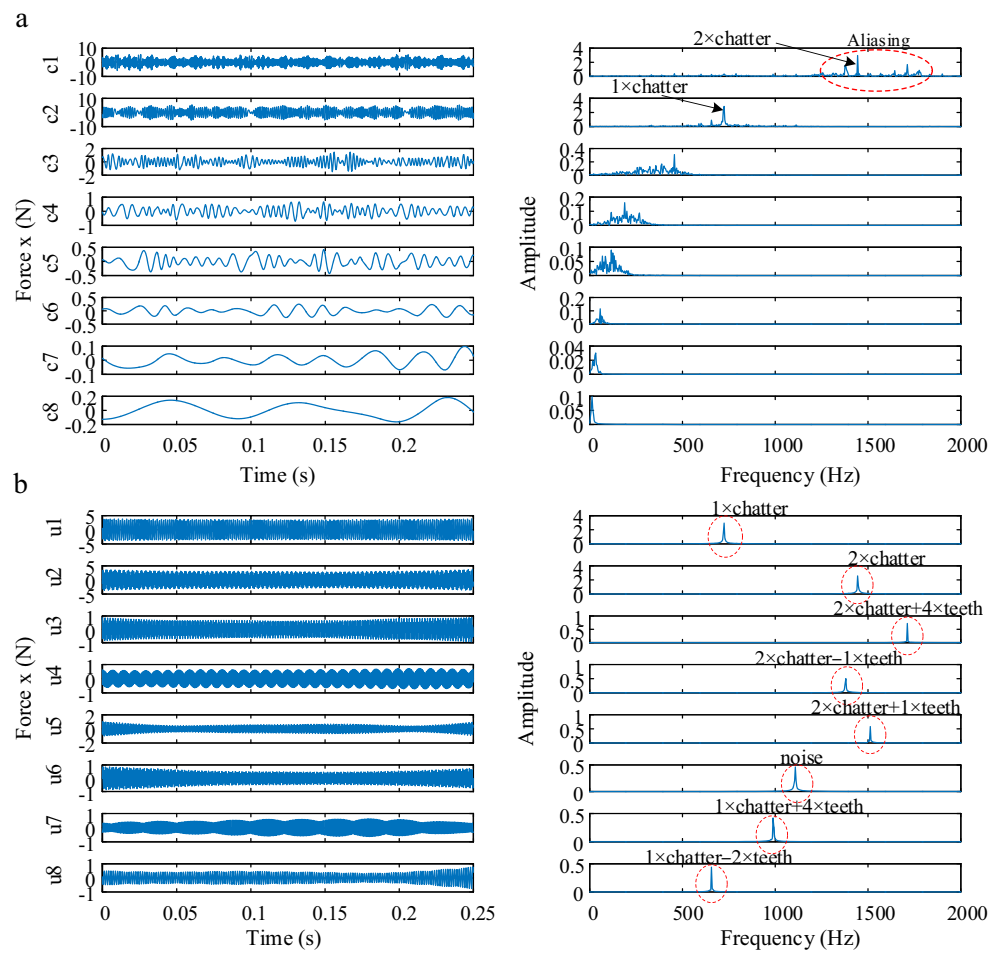




**Fig. 20** Signal decompositions of sample 3 in Fig. 19. **a** By the EMD. **b** By the I-VKF (both after the pre-filtering by the VKF)



EMD is used, because the collected signal contains noise that is inevitable in engineering. Based on the I-VKF, the harmonic-like components have been recovered from the noisy signal, which makes the characteristic peaks of chatter in the spectra conspicuous (see Fig. 20b). The superiority of the I-VKF over EMD is further shown in analyses of the energy distribution and energy entropy based on extracted single modes. As Fig. 21 and Fig. 22 show, three different cutting states cannot be distinguished by means of the EMD. This came as no surprise because an ineffective signal decomposition will render the subsequent computation of the chatter index ineffective too.

### 7 Conclusions

To protect the machine tool and workpiece from the damage caused by chatter, it is necessary to detect chatter timely and accurately in machining processes. Since the chatter can be characterized by the progressive variation in the energy distribution, when chatter occurs, the decreasing randomness of vibration responses can be captured by energy entropy, a generalization of Shannon’s entropy in the energy domain. To make such an index more sensitive to transitions of the cutting state, the energy entropy should be computed based on single signal modes that are obtained by means of signal

**Fig. 21** Energy distribution of single modes from test #5 signal in online experiment II. **a** Based on the EMD. **b** Based on the I-VKF

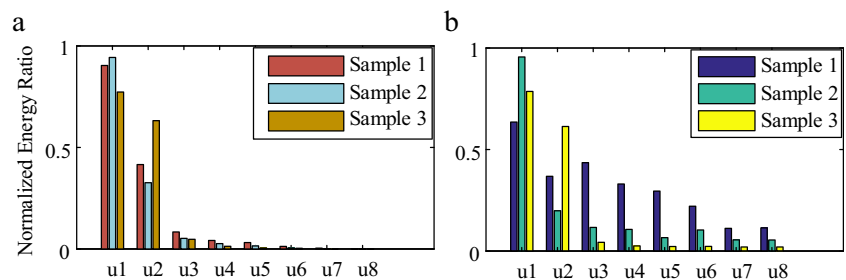
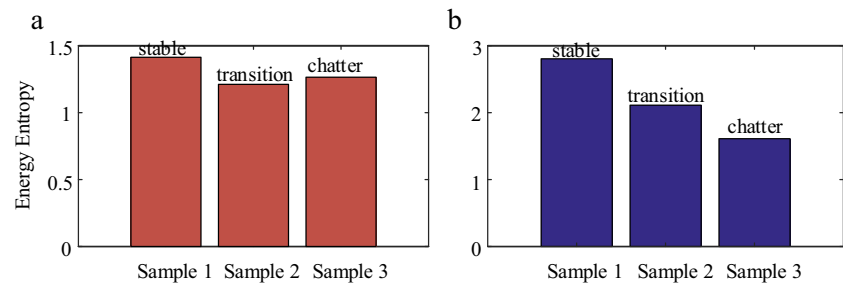


**Fig. 22** Energy entropy of each sample in experiment II. **a** Based on the EMD. **b** Based on the I-VKF



decompositions. Considering that the applications of the well-known EMD and VMD are limited due to the sensitivity to noise and the need for a priori information, respectively, the I-VKF is proposed in this work as an efficient multicomponent signal decomposition tool.

Based on the idea of the greedy algorithm, the original VKF, which adopts a joint optimization framework, is modified to recursively extract each chatter mode (i.e., signal modes are no longer simultaneously extracted). This modification improves the stability and adaptability of the filter, and does not increase the computational cost. In the meanwhile, a novel technique based on the SCI is developed to parametrically estimate the instantaneous chatter frequency of the dominant mode in the current signal, and thus to initiate each round of extraction. This technique transforms the estimation of a continuous IF into the optimization of a few polynomial parameters, which simplifies the problem and improves the robustness of the filter. As a result, the proposed I-VKF acts as an adaptive time-frequency filter and achieves much better performance than the EMD, VMD, and original VKF do, especially in the presence of strong noises, which has been verified by numerical examples.

By modeling the distribution of the energy entropy sample under stable cutting as a Gaussian type, we determine the alarm threshold of chatter through the maximum likelihood estimation and three-sigma criterion. With this threshold, an online chatter detection strategy is detailed. Through dynamic simulation and experimental verification, it has been demonstrated that chatter can be detected timely when the proposed strategy is used. The variation in entropy can be clearly observed during the transition from stable cutting to chatter. When other similar schemes such as the EMD-based entropy monitoring are employed, the decrease in the randomness of the collected signal cannot be revealed because the fundamental signal decomposition is ineffective in this case. Despite the fact that the focus of this work is milling chatter, the developed approach can be applied to other common machining operations such as turning and boring, because chatter in these processes can also be explained by the regenerative effect and be characterized by non-harmonic frequency components and decreasing entropy.

**Code availability** Thanks to MATLAB® for providing software support. Code will be made available on reasonable request.

**Author contribution** Xingjian Dong: funding acquisition and investigation. Guowei Tu: writing, methodology, and investigation. Xiaoshan Wang: writing, formal analysis, and investigation. Shiqian Chen: methodology and investigation.

**Funding** This work was supported by the National Natural Science Foundation of China (grant number 11872243).

**Data availability** Data will be made available on reasonable request.

## Declarations

**Ethics approval and consent to participate** The manuscript has not been submitted to any other journal for simultaneous consideration. The submitted work is original and has not been published elsewhere in any form or language. All authors participated in this research.

**Consent for publication** All authors agree to the publication of the paper.

**Conflict of interest** The authors declare no competing interests.

## References

- Quintana G, Ciurana J (2011) Chatter in machining processes: a review. *Int J Mach Tools Manuf* 51:363–376. <https://doi.org/10.1016/j.ijmachtools.2011.01.001>
- Budak E, Altintas Y (1998) Analytical prediction of chatter stability in milling—part I: general formulation. *J Dyn Syst Meas Control* 120:22–30. <https://doi.org/10.1115/1.2801317>
- Huang P, Li J, Sun J, Zhou J (2013) Vibration analysis in milling titanium alloy based on signal processing of cutting force. *Int J Adv Manuf Technol* 64:613–621. <https://doi.org/10.1007/s00170-012-4039-x>
- Hynynen KM, Ratava J, Lindh T, Rikkonen M, Ryyänen V, Lohtander M, Varis J (2014) Chatter detection in turning processes using coherence of acceleration and audio signals. *J Manuf Sci Eng* 136. <https://doi.org/10.1115/1.4026948>
- Kuljanic E, Totis G, Sortino M (2009) Development of an intelligent multisensor chatter detection system in milling. *Mech Syst Signal Process* 23:1704–1718. <https://doi.org/10.1016/j.ymssp.2009.01.003>

6. Ma H, Wu J, Yang L, Xiong Z (2017) Active chatter suppression with displacement-only measurement in turning process. *J Sound Vib* 401:255–267. <https://doi.org/10.1016/j.jsv.2017.05.009>
7. Tsai NC, Chen DC, Lee RM (2010) Chatter prevention for milling process by acoustic signal feedback. *Int J Adv Manuf Technol* 47:1013–1021. <https://doi.org/10.1007/s00170-009-2245-y>
8. Pérez-Canales D, Vela-Martínez L, Carlos Jáuregui-Correa J, Alvarez-Ramirez J (2012) Analysis of the entropy randomness index for machining chatter detection. *Int J Mach Tools Manuf* 62:39–45. <https://doi.org/10.1016/j.ijmactools.2012.06.007>
9. Li K, He S, Li B, Liu H, Mao X, Shi C (2020) A novel online chatter detection method in milling process based on multiscale entropy and gradient tree boosting. *Mech Syst Signal Process* 135:106385. <https://doi.org/10.1016/j.ymsp.2019.106385>
10. Liu Y, Wang X, Lin J, Kong X (2020) An adaptive grinding chatter detection method considering the chatter frequency shift characteristic. *Mech Syst Signal Process* 142:106672. <https://doi.org/10.1016/j.ymsp.2020.106672>
11. Chen ZZ, Li ZL, Niu JB, Zhu LM (2020) Chatter detection in milling processes using frequency-domain Rényi entropy. *Int J Adv Manuf Technol* 106:877–890. <https://doi.org/10.1007/s00170-019-04639-5>
12. Huang NE, Shen Z, Long SR, Wu MC, Shih HH, Zheng Q, Yen N-C, Tung CC, Liu HH (1998) The empirical mode decomposition and the Hilbert spectrum for nonlinear and non-stationary time series analysis. *Proc R Soc London Ser A Math Phys Eng Sci* 454:903–995. <https://doi.org/10.1098/rspa.1998.0193>
13. Shrivastava Y, Singh B (2019) A comparative study of EMD and EEMD approaches for identifying chatter frequency in CNC turning. *Eur J Mech - A/Solids* 73:381–393. <https://doi.org/10.1016/j.euromechsol.2018.10.004>
14. Dragomiretskiy K, Zosso D (2014) Variational mode decomposition. *IEEE Trans Signal Process* 62:531–544. <https://doi.org/10.1109/TSP.2013.2288675>
15. Liu C, Zhu L, Ni C (2018) Chatter detection in milling process based on VMD and energy entropy. *Mech Syst Signal Process* 105:169–182. <https://doi.org/10.1016/j.ymsp.2017.11.046>
16. Tu G, Dong X, Chen S, Zhao B, Hu L, Peng Z (2020) Iterative nonlinear chirp mode decomposition: a Hilbert-Huang transform-like method in capturing intra-wave modulations of nonlinear responses. *J Sound Vib* 485:115571. <https://doi.org/10.1016/j.jsv.2020.115571>
17. Tu G, Dong X, Qian C, Chen S, Hu L, Peng Z (2021) Intra-wave modulations in milling processes. *Int J Mach Tools Manuf* 103705. <https://doi.org/10.1016/j.ijmactools.2021.103705>
18. Gilles J (2013) Empirical wavelet transform. *IEEE Trans Signal Process* 61:3999–4010. <https://doi.org/10.1109/TSP.2013.2265222>
19. Chen S, Wang K, Peng Z, Chang C, Zhai W (2021) Generalized dispersive mode decomposition: algorithm and applications. *J Sound Vib* 492:115800. <https://doi.org/10.1016/j.jsv.2020.115800>
20. Chen S, Wang K, Chang C, Xie B, Zhai W (2021) A two-level adaptive chirp mode decomposition method for the railway wheel flat detection under variable-speed conditions. *J Sound Vib* 498:115963. <https://doi.org/10.1016/j.jsv.2021.115963>
21. Zhao B, Cheng C, Tu G, Peng Z, He Q, Meng G (2021) An interpretable denoising layer for neural networks based on reproducing kernel Hilbert space and its application in machine fault diagnosis. *Chinese J Mech Eng* 34:44. <https://doi.org/10.1186/s10033-021-00564-5>
22. Vold H, Leuridan J (1993) High resolution order tracking at extreme slew rates, using Kalman tracking filters. SAE Technical Paper. SAE International
23. Kalman RE (1960) A new approach to linear filtering and prediction problems. *J Basic Eng* 82:35–45. <https://doi.org/10.1115/1.3662552>
24. Insperger T, Stépán G, Bayly P, Mann B (2003) Multiple chatter frequencies in milling processes. *J Sound Vib* 262:333–345. [https://doi.org/10.1016/S0022-460X\(02\)01131-8](https://doi.org/10.1016/S0022-460X(02)01131-8)
25. Pan MC, Lin YF (2006) Further exploration of Vold-Kalman-filtering order tracking with shaft-speed information - I: theoretical part, numerical implementation and parameter investigations. *Mech Syst Signal Process* 20:1134–1154. <https://doi.org/10.1016/j.ymsp.2005.01.005>
26. Yang Y, Peng Z, Dong X, Zhang W, Meng G (2014) Application of parameterized time-frequency analysis on multicomponent frequency modulated signals. *IEEE Trans Instrum Meas* 63:3169–3180. <https://doi.org/10.1109/TIM.2014.2313961>
27. Yu Y, YuDejie JC (2006) A roller bearing fault diagnosis method based on EMD energy entropy and ANN. *J Sound Vib* 294:269–277. <https://doi.org/10.1016/j.jsv.2005.11.002>
28. Shannon CE (1948) A mathematical theory of communication. *Bell Syst Tech J* 27:379–423. <https://doi.org/10.1002/j.1538-7305.1948.tb01338.x>
29. Vela-Martínez L, Carlos Jáuregui-Correa J, Rodríguez E, Alvarez-Ramirez J (2010) Using detrended fluctuation analysis to monitor chattering in cutter tool machines. *Int J Mach Tools Manuf* 50:651–657. <https://doi.org/10.1016/j.ijmactools.2010.03.012>
30. Myung IJ (2003) Tutorial on maximum likelihood estimation. *J Math Psychol* 47:90–100. [https://doi.org/10.1016/S0022-2496\(02\)00028-7](https://doi.org/10.1016/S0022-2496(02)00028-7)
31. Pukelsheim (1994) The three sigma rule. *Am Stat* 48:88–91. <https://doi.org/10.1080/00031305.1994.10476030>
32. Kennedy J, Eberhart R (1995) Particle swarm optimization. In: *Proceedings of ICNN'95 - International Conference on Neural Networks*. pp 1942–1948 vol.4
33. Yang X, Yuan J, Yuan J, Mao H (2007) A modified particle swarm optimizer with dynamic adaptation. *Appl Math Comput* 189:1205–1213. <https://doi.org/10.1016/j.amc.2006.12.045>
34. Tuma J (2005) Setting the passband width in the Vold-Kalman order tracking filter. *12th Int Congr Sound Vib 2005, ICSV 2005* 5:4357–4364
35. Flandrin P, Rilling G, Goncalves P (2004) Empirical mode decomposition as a filter bank. *IEEE Signal Process Lett* 11:112–114. <https://doi.org/10.1109/LSP.2003.821662>
36. Wang Y, Markert R (2016) Filter bank property of variational mode decomposition and its applications. *Signal Process* 120:509–521. <https://doi.org/10.1016/j.sigpro.2015.09.041>
37. Nair U, Krishna BM, Namboothiri VNN, Nampoori VPN (2010) Permutation entropy based real-time chatter detection using audio signal in turning process. *Int J Adv Manuf Technol* 46:61–68. <https://doi.org/10.1007/s00170-009-2075-y>
38. Pérez-Canales D, Álvarez-Ramírez J, Jáuregui-Correa JC, Vela-Martínez L, Herrera-Ruiz G (2011) Identification of dynamic instabilities in machining process using the approximate entropy method. *Int J Mach Tools Manuf* 51:556–564. <https://doi.org/10.1016/j.ijmactools.2011.02.004>
39. Balachandran B (2001) Nonlinear dynamics of milling processes. *Philos Trans R Soc London Ser A Math Phys Eng Sci* 359:793–819. <https://doi.org/10.1098/rsta.2000.0755>
40. Faassen RPH, van de Wouw N, Oosterling JAJ, Nijmeijer H (2003) Prediction of regenerative chatter by modelling and analysis of high-speed milling. *Int J Mach Tools Manuf* 43:1437–1446. [https://doi.org/10.1016/S0890-6955\(03\)00171-8](https://doi.org/10.1016/S0890-6955(03)00171-8)
41. Yao Z, Mei D, Chen Z (2010) On-line chatter detection and identification based on wavelet and support vector machine. *J Mater Process Technol* 210:713–719. <https://doi.org/10.1016/j.jmatprotec.2009.11.007>
42. Li Y, Liu S, Shu L (2019) Wind turbine fault diagnosis based on Gaussian process classifiers applied to operational data. *Renew Energy* 134:357–366. <https://doi.org/10.1016/j.renene.2018.10.088>

43. Wang GF, Li YB, Luo ZG (2009) Fault classification of rolling bearing based on reconstructed phase space and Gaussian mixture model. *J Sound Vib* 323:1077–1089. <https://doi.org/10.1016/j.jsv.2009.01.003>
44. Glowacz A, Glowacz W, Glowacz Z, Kozik J (2018) Early fault diagnosis of bearing and stator faults of the single-phase induction motor using acoustic signals. *Measurement* 113:1–9. <https://doi.org/10.1016/j.measurement.2017.08.036>
45. Lilliefors HW (1967) On the Kolmogorov-Smirnov test for normality with mean and variance unknown. *J Am Stat Assoc* 62:399–402. <https://doi.org/10.1080/01621459.1967.10482916>
46. Dallal GE, Wilkinson L (1986) An analytic approximation to the distribution of Lilliefors's test statistic for normality. *Am Stat* 40: 294–296. <https://doi.org/10.1080/00031305.1986.10475419>
47. Kuljanic E, Sortino M, Totis G (2008) Multisensor approaches for chatter detection in milling. *J Sound Vib* 312:672–693. <https://doi.org/10.1016/j.jsv.2007.11.006>

**Publisher's note** Springer Nature remains neutral with regard to jurisdictional claims in published maps and institutional affiliations.